Applied Water Science (2023) 13:152
https://doi.org/10.1007/s13201-023-01955-w

ORIGINAL ARTICLE

Modification of graphene oxide with imidazolium-based ionic liquid for significant sorption of La(III) and Pr(III) from aqueous solutions

Elsayed Mustafa Abu Elgoud[1] · Ahmed Ibrahim Abd-Elhamid[2] · Hisham Fouad Aly[1]

Received: 29 September 2022 / Accepted: 23 May 2023 / Published online: 12 June 2023

Abstract

A straightforward ferrocyanide immobilization on the surface of graphene oxide (GO) was conducted for rapid and efficient adsorption capacity for lanthanum and praseodymium from an aqueous solution. The GO was mixed with 1-methyl imidazole in the presence of epichlorohydrin to form GO-imidazole-Cl and thereafter suspended in a potassium ferrocyanide solution to fabricate GO-imidazole-FeCN. The prepared materials were characterized with different advanced techniques confirming the preparation method. The adsorption ability of GO-imidazole-FeCN towards La(III) and Pr(III) ions was evaluated. Moreover, the adsorption isotherm showed that the sorption process was fitted with the Langmuir isotherm model with a considerable maximum adsorption capacity of 781.25 mg g^{-1} for La(III) and 862.07 mg g^{-1} for Pr(III). The thermodynamic studies showed that the adsorption of both metal ions was spontaneous and endothermic. In addition, the adsorbent showed excellent adsorption–desorption behavior over 5 times, suggesting that GO-imidazole-FeCN may be considered a potential candidate for La(III) and Pr(III) removal from different metal ions which present in fission products.

Keywords GO · Imidazole · Potassium ferrocyanide · Composite · Lanthanum · Praseodymium

Introduction

Lanthanide elements are one of the significant fission products which are generated from irradiated nuclear fuel. The environmental conduct of lanthanide elements has received a significant advantage in the environmental impact assessment of disposed long-lived radioactive waste (Behdani et al. 2013; Zuo et al. 2011). Over the past decades, due to their unique magnetic, catalytic, electronic, and optical properties, lanthanide elements have been increasingly applied in energy-saving and renewable energy technologies, from solar panels and electric vehicle batteries to high-execution magnets (Xu and Qu 2014; Ronda et al. 1998). The development of clean energy will increase the demand for these technologically advanced materials.

Lanthanum is one of the most abundant and reactive elements among lanthanides. It is widely used in various applications, such as catalysts, super-alloys, optical glasses, organic synthesis, and special ceramics (Tadjarodi et al. 2015). Praseodymium is employed in magnetic materials, coloring materials, hydrogen storage materials, refractory substances, lighting equipment, fiber optical cables, advanced alloys, and battery materials (Zhang et al. 2014). The uses of lanthanum and praseodymium in different industries lead to significant concern about their release of wastewater effluents into aquatic and soil environments. On the other hand, the adsorption of lanthanum and praseodymium has been the objective of several investigations on different adsorbents due to their relevance as fission products in radioactive waste. Different adsorbents have been applied for the adsorption of lanthanum and praseodymium. For example, Zhao et al. 2021, modified GO with tris(4-aminophenyl) amine composites (GO-$TAPA_{1:2}$ composite) for extracting some rare earth elements from

✉ Ahmed Ibrahim Abd-Elhamid
ahm_ch_ibr@yahoo.com

Elsayed Mustafa Abu Elgoud
elsayedmustafa36@yahoo.com

Hisham Fouad Aly
alydrhisham@yahoo.com

[1] Hot Laboratories Center, Egyptian Atomic Energy Authority, Nasr City 13759, Egypt

[2] Composites and Nanostructured Materials Research Department, Advanced Technology and New Materials Research Institute (ATNMRI), City of Scientific Research and Technological Applications (SRTA-City), New Borg Al-Arab, Alexandria 21934, Egypt

an aqueous solution. Sayed et al. 2021 employed nanogoethite (NG), activated carbon-modified goethite (GAC-1), and sodium alginate-modified goethite (GSA-2) for the sorption of lanthanum from aqueous media. Furthermore, Gaete et al. 2021 studied the adsorption of La(III), Pr(III), and Sm(III) from an aqueous solution using magnetic nanoparticles loaded with a phosphonic acid group (PA-MNPs). Liu et al. (2019) selectively removed La(III) by employing two bio-templated chiral nematic mesoporous silica films (MSFs). Najafi et al. (2018) prepared chitosan/polyvinyl alcohol/3-mercaptopropyltrimethoxysilane (CTS/PVA/TMPTMS) beads for adsorption of La(III) and Ce(III). Ashour et al. (2017) studied the adsorption behavior of GO nanosheets for the sorption of some rare earth elements. Su et al. (2014) synthesized Fe_3O_4@SiO_2@polyaniline-graphene oxide to recover La(III) and Pr(III). He et al. (2021) prepared an algal biomass/ polyethyleneimine (PEI) composite for the effective sorption of Pr(III) and Tm(III) from mining residues. Devanathan et al. (2021) prepared a hydrophobic ionic liquid based on D-galactose (IL5) for the removal of Ce(III) and Pr(III) ions from solutions. In addition, Rangabhashiyam et al. (2021) examined polysulfone immobilized with Turbinaria conoides (PITC) for the removal of Pr(III) and Tm(III) from mono and binary solutions. Stashkiv et al. (2019) investigated the adsorption of Pr(III) by using the Transcarpathian Clinoptilolite. Bendia et al. (2017) employed polyethyleneimine sodium phosphonate resin (PEIPR-Na) for the recovery and separation of La(III), Pr(III), and U(VI) from aqueous solution. Xiong et al. (2012) estimated the behavior of D72 Resin for Pr(III) sorption from an aqueous solution.

Ionic liquids have been widely utilized in separating and extracting some radionuclides due to their high chemical and thermal stability, tunable structure, and good radiation resistance (Favre-Reguillon et al. 2019; Pepper and Ogden 2013; Zsabka et al. 2018). Imidazolium-based ionic liquids are one of the most significant categories of ionic liquids. They possess many advantages, such as thermal stability, water-soluble, non-toxic, biodegradable, high sorption of some metals, and high protection efficiency (Subasree and Selvi 2020; Singh et al. 2018). Furthermore, the low utilization rate, high cost, and difficulty in recycling ionic liquids into the extraction and separation processes limit their further application. Many studies demonstrated that impregnating ionic liquids on a suitable solid material improves the sorption and separation of some organic and inorganic pollutants from the aqueous solution (Xie et al. 2021; Xin and Hao 2014; Zhao et al. 2016). Previously, several studies reported that ionic liquids immobilized on various organic and inorganic solids such as magnetic polymers (Liu et al. 2022), silica nanoparticles (Lei et al. 2022), magnetic nanoparticles (Naushad et al. 2021), cellulose microsphere (Dong and Zhao 2018), and chitosan (Lou et al. 2018).

Graphene oxide is a layered material with a high density of different oxygen functional groups (–OH, C=O, C–O–C, and COOH) that decorate its surface and edges. Although the presence of all of these active groups, in the present study, the GO exhibited low performance in the adsorption of both La(III) and Pr(III) from aqueous solutions. Therefore, we examined surface modification of the GO with 1-methyl imidazole and epichlorohydrin as a linker to construct (GO-imidazole-Cl), which also showed low adsorption efficiencies towards La(III) and Pr(III). Thus, in this investigation, Cl^- ion in (GO-imidazole-Cl) was replaced with $K_3[Fe(CN)_6]^-$ anion through a reaction with $K_4[Fe(CN)_6]$ to form (GO-imidazole-FeCN), which exhibits significant adsorption affinity higher than (GO and GO-imidazole-Cl) towards La(III) and Pr(III). Moreover, the influence of different parameters, including contact time, solution pH, metal ion concentration, adsorbent dosage, and temperature, on the sorption process was investigated. The synthesized GO-imidazole-FeCN composite was characterized using TEM, EDX mapping, SEM, XRD, FTIR, and Raman before and after adsorption.

Experimental

Materials and instrumentation (Supplementary Materials)

GO-imidazole-Cl

The GO-imidazole-Cl was prepared through a simple route as follows: Firstly, GO (150 mg) was dispersed in 1L double distilled water. Secondly, 10 mL (1-methyl imidazole) was added to the GO suspension. Thirdly, 20 mL epichlorohydrin (ECH) was added dropwise to the previous mixture and kept stirring at two different temperatures (50 °C for 24 h) and (90 °C for another 24 h). Finally, the solid was separated by filtration, washed several times with double distilled water, and stored for further usage.

GO-imidazole-FeCN

GO-imidazole-FeCN was further prepared according to Scheme 1, where 600 mg of GO-imidazole-Cl was added to 1L (2% w/v) aqueous solution of $K_4[Fe(CN)_6]$ and stirred at 70 °C for 24 h.

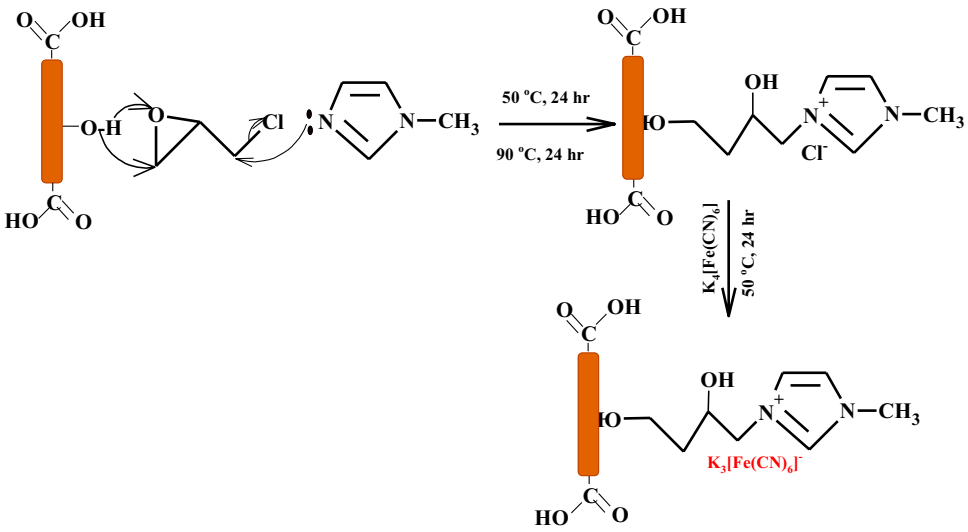

Scheme 1 Schematic presentation of preparation procedure of GO-imidazole-FeCN

Characterizations (Supplementary Materials)

Batch adsorption studies (Supplementary Materials)

Mathematical models (Supplementary Materials)

Results and discussion

Characterization

SEM and TEM

The SEM and TEM micrographs of GO-imidazole-Cl (Fig. 1a–f, respectively) and GO-imidazole-FeCN (Fig. 1g–l, respectively), GO-imidazole-FeCN-La (Fig. S1a–f, respectively) and GO-imidazole-FeCN-Pr (Fig. S1g–l, respectively) are shown. The images showed that all the previously characterized species presented as flat and separated layered structures. This implies that the binding sites of the adsorbents (GO-imidazole-Cl & GO-imidazole-FeCN) were presented in a suitable location that allowed them to interact successfully with the contaminated species quickly and effectively. In contrast, the layered flat structure of the (GO-imidazole-FeCN-La & GO-imidazole-FeCN-Pr) will induce a fast and effective regeneration process of the used adsorbent.

EDX elemental mapping and analysis

The GO is mainly composed of C and O. After the modification of GO with 1-methyl imidazole to form GO-imidazole-Cl, the STEM image and related EDX elemental mapping images obtained from their K-lines, Fig. 2a–e, clearly revealed uniform distribution of *N* (1-methyl imidazole) and Cl (EPC) in the GO-layer. This induces a successful modification reaction, and the Cl was substituted by $K_4[Fe(CN)_6]$ to compose GO-imidazole-FeCN (Fig. 2f–k). Hence, the mapping analysis showed the absence of Cl, high density of the N, and appearance of K and Fe, affirming successful substitution reaction.

FTIR The FTIR spectra of GO, GO-imidazole-Cl, GO-imidazole-FeCN (Fig. 3a). The GO FTIR spectra present four main bands at 3214, 1721, 1620, and 1031 cm^{-1} for adsorbed water (COOH) group correspondence, H_2O stretching, and C–O stretching, respectively. After the reaction of GO with EPC and imidazole, the FTIR spectrum of GO-imidazole-Cl was altered from the GO spectrum, see Fig. 3a, the bands at 3214, 1721 and 1031 cm^{-1} (for GO) were shifted to 3313, 1708 and 1029 cm^{-1} (for GO-imidazole-Cl) after the modification process. In addition, the band at 1620 cm^{-1} completely disappeared, and new bands at 1570 and 1162 cm^{-1}, corresponding to C = C stretching of cyclic alkene (Barroso-Bogeat et al. 2019) and C–O–C stretching (Baranitharan et al. 2019), respectively. By treating the GO-imidazole-Cl with $K_4[Fe(CN)_6]$ to fabricate GO-imidazole-FeCN the bands at 3313, 1708, 1162 and 1029 cm^{-1} disappeared, while the band at 1570 cm^{-1} was shifted to 1520 cm^{-1}. Finally, a new weak band at 2204 cm^{-1} corresponding to the C≡N group appeared. These results revealed that the Cl^- was successfully replaced by $K_3[Fe(CN)_6]^-$.

Raman

The Raman spectra of GO, GO-imidazole-Cl, and GO-imidazole-FeCN (Fig. 3b) reflected two main bands: D-band

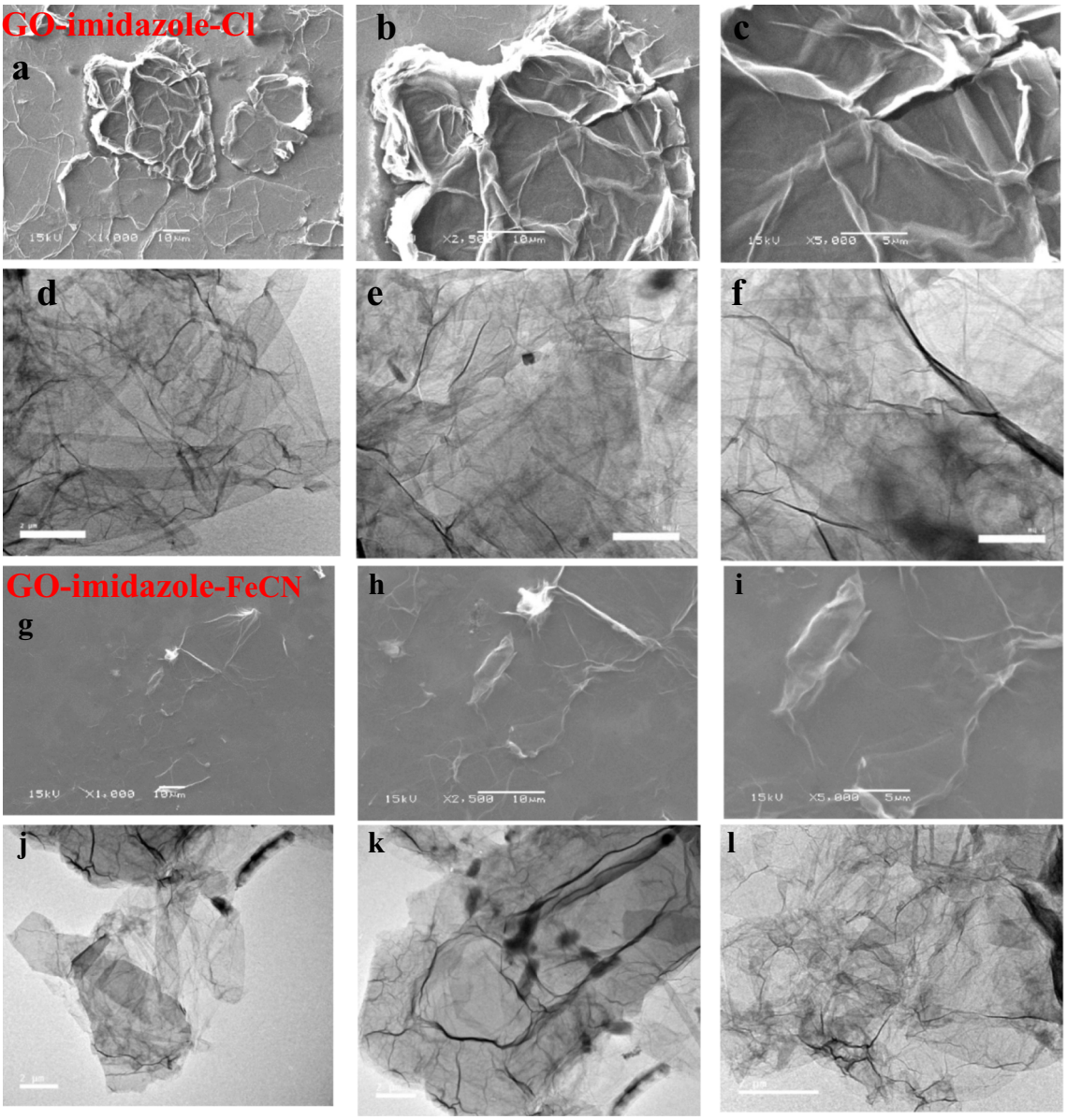

Fig. 1 SEM and TEM images for GO-imidazole-Cl and GO-imidazole-FeCN

(detect the defective degree) and G-band (describe the in-plane C–C bond stretching) (Huo et al. 2021). After the GO modification process, there was a reduction in the intensity ratio of I_D/I_G from 1.32 (GO) to 1.27 (GO-imidazole-Cl) and to 1.11 (GO-imidazole-FeCN), indicating a decrease in defect degree in the GO sheet. This may be attributed to the functionalization process.

TGA analysis

The thermogravimetric analysis is considered an efficient tool for the thermal stability of the analyzed materials. The TGA was applied to identify the different thermal weight loss stages associated with GO and GO-imidazole-FeCN, see Fig. 3c. The GO showed five degradation steps due to: evaporation of adsorbed surface water (28–88 °C, 19.6%), the liberation of interlayer water (88–158 °C, 4.07%), decomposition of oxygen functional groups (158–215 °C, 4.07%) and pyrolysis of carbon skeleton (215–320 °C, 8.40%) (Fig. 3c). Compared with GO, the GO-imidazole-FeCN possesses high thermal stability over all various thermal decomposition stages (at the same decomposition temperature range) (Fig. 3c). This may be because most of the oxygenated functional groups on both sides of the GO-layer (which will be co-responsible for H-bonding with the surface water) were contributed in the modification step.

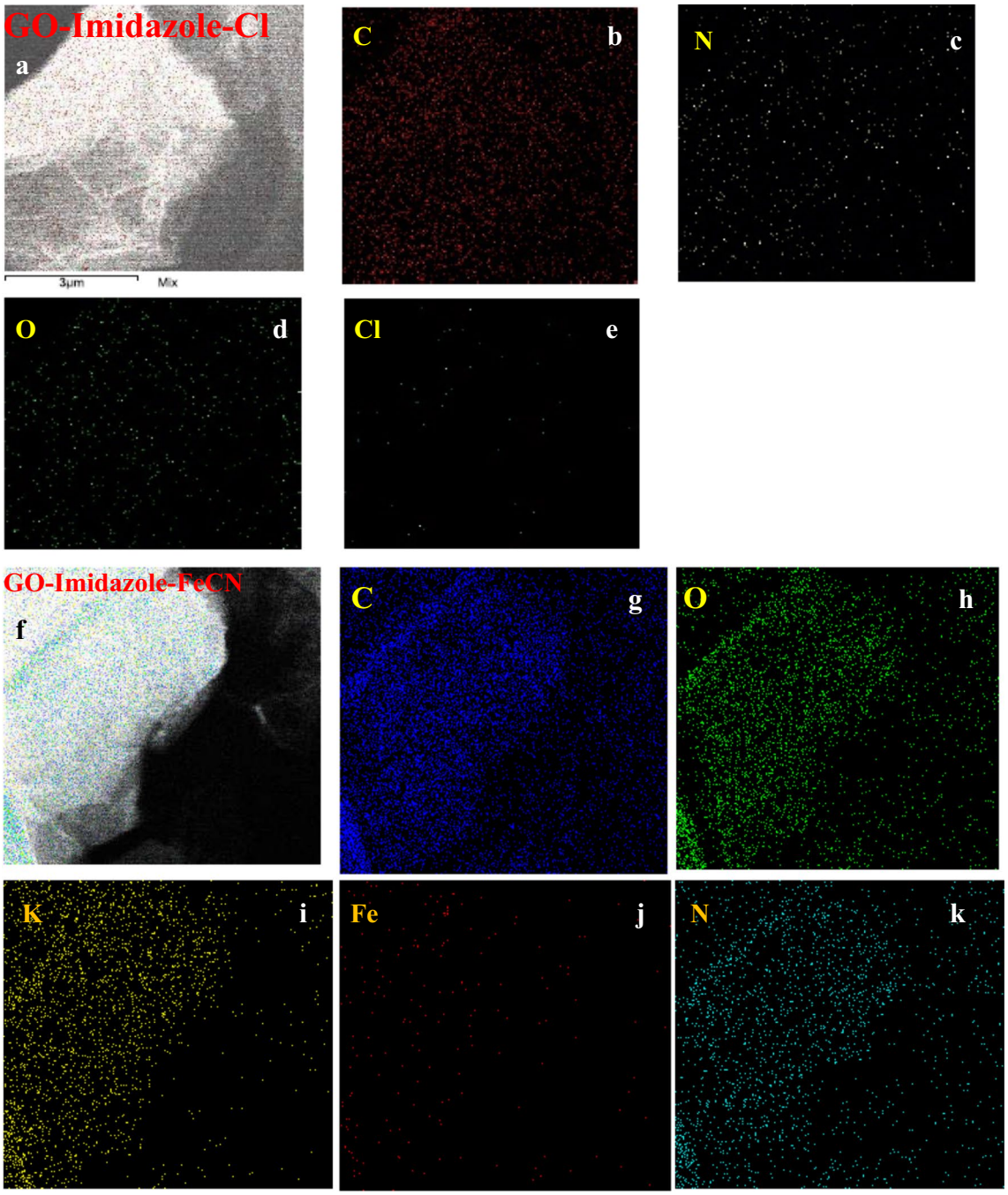

Fig. 2 STEM image and EDX mapping of **a**–**e** GO-imidazole-Cl and **f**–**k** GO-imidazole-FeCN

Consequently, the amount of the adsorbed surface water will be reduced, and the oxygen groups will be shielded.

EDS analysis

EDS is a valuable device employed for assessing the elements constructer of the materials. The EDS analysis of GO-imidazole-Cl, GO-imidazole-Fe(CN), GO-imidazole-Fe(CN)-La, and GO-imidazole-Fe(CN)-Pr were conducted as described in Fig. S2. The EDS analysis of GO-imidazole-Cl showed C (GO, ECH, 2-MI), O (GO, ECH), N (2-MI), and Cl (ECH), as presented in Fig. S2a. By mixing GO-imidazole-Cl with $K_4[Fe(CN)_6]$, a reduction in Cl percentage was observed. The appearance of new elements, like K and Fe ($K_4[Fe(CN)_6]$) which confirm the substitution reaction and formation of GO-imidazole-Fe(CN), see Fig. S2b. After the adsorption step, the EDS analysis was performed to evaluate the successful sorption of La(III) and Pr(III) ions

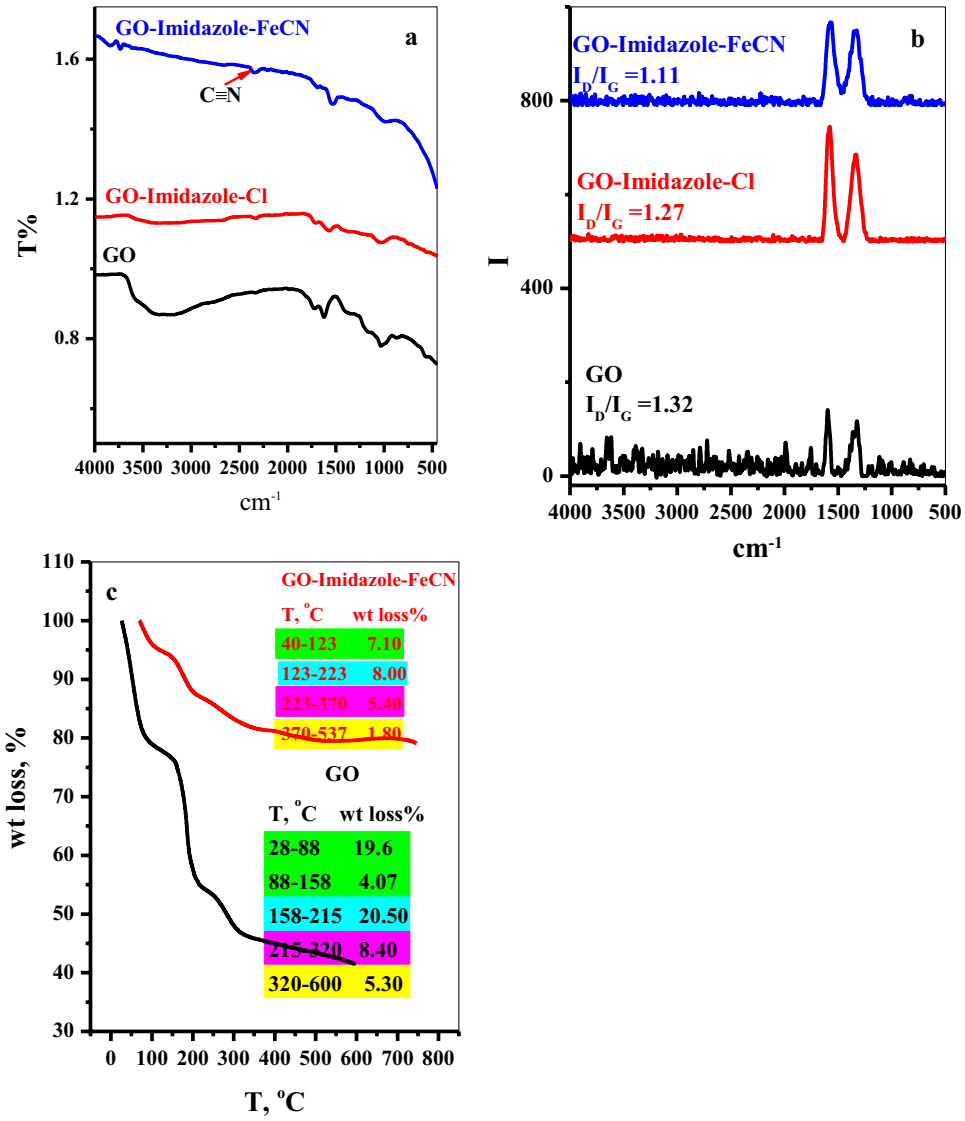

Fig. 3 **a** FTIR spectrum, **b** Raman spectrum of GO, GO-imidazole-Cl and GO-imidazole-FeCN and **c** Thermogravimetric diagram of GO and GO-imidazole-FeCN composite

on the GO-imidazole-Fe(CN). The obtained data reflected the existence of new peaks of La(III) (Fig. S2c) and Pr(III) (Fig. S2d) with a reduction of K%, indicating that the La and Pr adsorption process proceeded through K-cation exchange.

Adsorption investigation

Effect of contact time

The induce of mixing time on the remediation ability of the GO, GO-imidazole-Cl, and GO-imidazole-FeCN towards La(III) and Pr(III) was investigated, as presented in Fig. 4a. It was observed that for all used adsorbents, both La(III) and Pr(III) were rapidly adsorbed at the first minute (in order GO-imidazole-Cl < GO < GO-imidazole-FeCN), behind it no further increase in the adsorption performance till 30 min, as shown in Fig. 4a. This observation is attributed to the GO, GO-imidazole-Cl, and GO-imidazole-FeCN, which have well-separated-sheets-like structure, which keep the active sites exposed to an aqueous solution. Consequently, the pollutant ion easily reaches the binding sites and interacts with the function group. However, the GO-imidazole-FeCN recorded the best adsorption efficiency among the used adsorbent. Therefore, GO-imidazole-FeCN was used for further experimental investigations.

To kinetically study these observations, the pseudo-second-order (PSO) kinetic equation was applied (see Table S1). The relation coefficient and the other measured parameters (K_2 and $q_{e\,cal}$) from the linear (t/q_t vs t) plot (Fig. S3a) are listed in Table S2. It is noted that ($R^2 = 0.999$) close to unit and the values of the calculated adsorption capacities ($q_{e\,cal,}$ mg/g) were greatly close to the adsorption capacity values measured from experiments (q_{exp}, mg/g). Therefore, we supposed that the adsorption kinetics followed the PSO

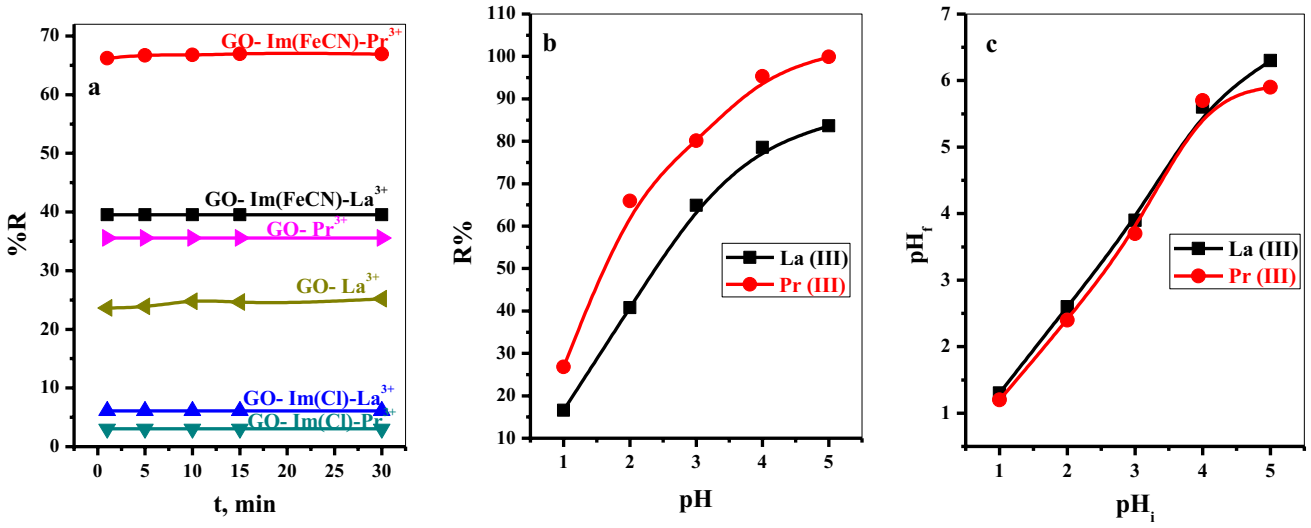

Fig. 4 **a** Effect of contact time on sorption percent of La(III) ($[La^{3+}]=50$ mg L^{-1}, dose = 1.0 mg, v = 5 mL, pH = 2, T = 25 ℃) and Pr(III) ($[Pr^{3+}]=50$ mg L^{-1}, dose = 1.0 mg, v = 5 mL, pH = 2, T = 25 ℃) from aqueous media. Effect of the initial solution pH on **b** the sorption percent, **c** final solution pH of the GO-imidazole-FeCN adsorbent of La(III) (t = 1 min, $[La^{3+}]=50$ mg L^{-1}, dose = 1 mg, v = 5 mL, T = 25 ℃) and Pr(III) (t = 1 min, $[Pr^{3+}]=50$ mg L^{-1}, dose = 1 mg, v = 5 mL, T = 25 ℃) from aqueous media

model, and the adsorption rate was mainly explained via the chemical adsorption process.

Effect of adsorption solution pH

Besides other parameters, pH plays a vital role in the adsorption process, where the pH values of the aqueous solution significantly induce both surface charges of adsorbent and adsorbate. Figure 4b presents the effect of the solution pH values on the removal rate of La(III) and Pr(III) on GO-imidazole-FeCN. It was found that the increase in the pH value from 1.0 to 5.0 is followed by a linear increase in the sorption efficiency of (La(III) from 16.56 to 83.62% and (Pr(III) from 26.81 to 99.9%.

Moreover, a linear increase in the final pH of the adsorption solution for both La(III) and Pr(III) was noted, as shown in Fig. 4c. This observation could be explained by the fact that the adsorption of the M-ion led to the release of the K-atoms into the bulk of the solution. This observation was confirmed by following the presence of iron and potassium in the solution after the adsorption process. The presence of potassium ions was noted in the adsorption solution. This released potassium can form KOH in the aqueous solution, which enhances the value of the pH of the solution.

Effect of initial metal ion concentration

Various initial concentrations of La(III) and Pr(III) in the range of 50.0–500.0 mg L^{-1} were applied to examine the adsorption properties of the GO-imidazole-FeCN. The obtained adsorption data are plotted in Fig. 5a. It can be noted that the adsorption rate keeps reducing with the further increase in the initial ions' concentrations. This phenomenon could be described by the fact that at low initial concentrations of the metal ion, a sufficient number of binding sites are available to interact with the ion species, whereas as the initial concentration of ions increases, the number of ion species also increases compared to the number of binding sites. Therefore, the adsorption efficiency is reduced.

Moreover, numerous isotherm models (Table S1) were employed to assess the experimental data to describe the mechanism of interaction between the La(III) and Pr(III) ions and GO-N-FeCN (Fig. S3b-k). The factors and correlation coefficients related to the models were also measured and are summarized in Table 1. The Langmuir model was found to be the best isotherm model to describe the adsorption process, where the correlation coefficient ($R^2 > 0.98$) related to the Langmuir model was higher than that of other isotherm models, see Table 1. Moreover, according to the Langmuir model, the GO-N-FeCN achieved the maximum adsorption capacities for La(III), 781.25 mg g^{-1}, and Pr(III), 862.07 mg g^{-1}.

Effect of adsorbent dosage

The effect of induced GO-imidazole-FeCN adsorbent quantity in the range of 0.001–0.005 g on the uptake efficiency of La(III) and Pr(III) is presented in Fig. 5b. It is worth noting that the adsorption rate of both studied metal ions linearly improved with the adsorbate dose. This behavior could be explained by increasing the adsorbent dose; the density of

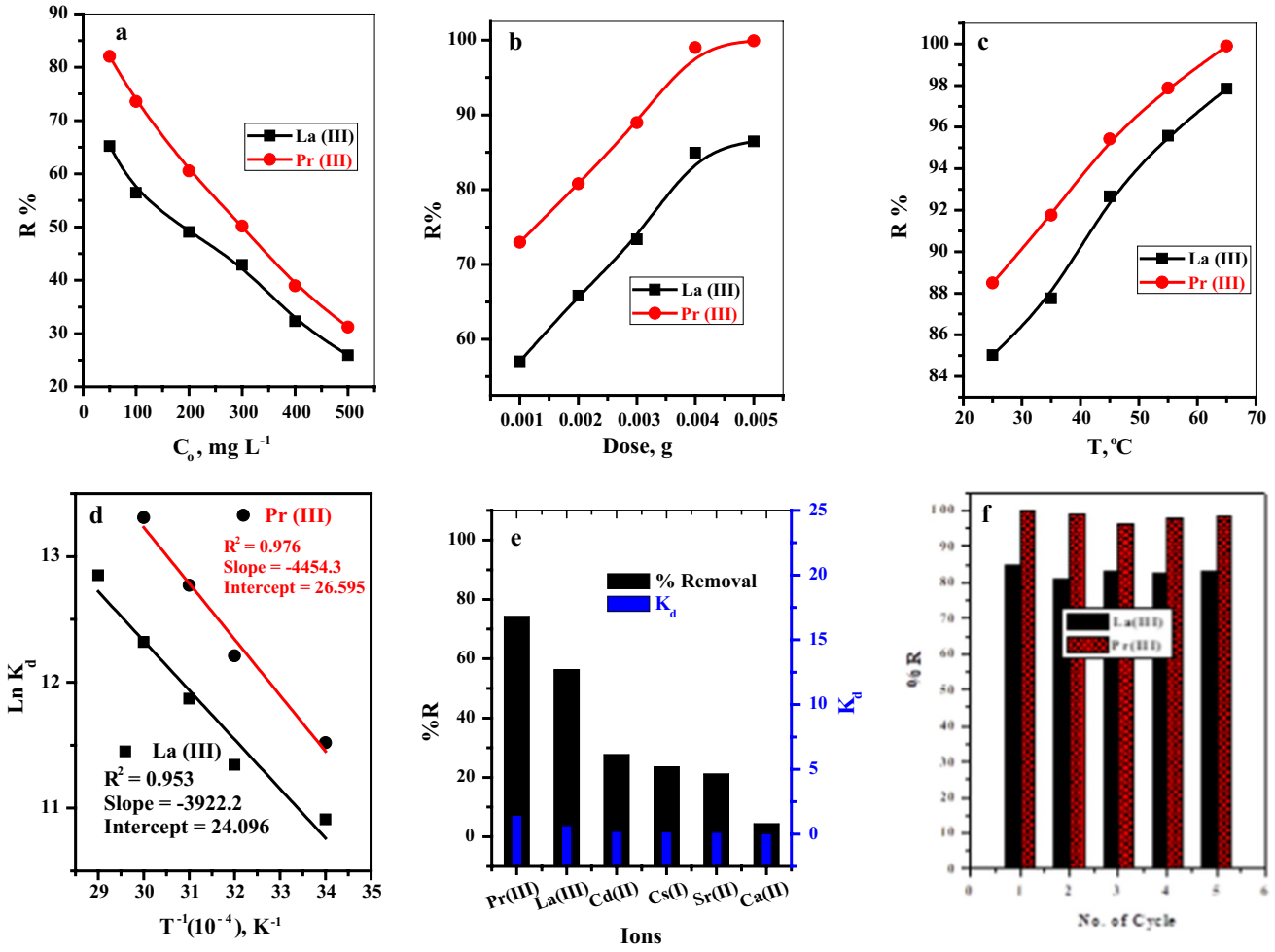

Fig. 5 **a** Effect of initial metal ion concentration on the sorption percent of La(III) and Pr(III) from aqueous media (t = 1 min, dose = 1 mg, v = 5 mL, pH = 3, T = 25 ℃) using GO-imidazole-FeCN. **b** Effects of adsorbent dosage on the sorption percent of La(III) (t = 1 min, [La^{3+}] = 100 mg L^{-1}, v = 5 mL, pH = 3, T = 25 ℃) and Pr(III) (t = 1 min, [Pr^{3+}] = 100 mg L^{-1}, v = 5 mL, pH = 3, T = 25 ℃) from aqueous media. Effect of **c** temperature on the sorption percent and d) thermodynamic parameters of La(III) (t = 1 min, [La] = 100 mg L^{-1}, dose = 4.0 mg, v = 5 mL, pH = 3, T = 25 ℃) and Pr(III) (t = 1 min, [Pr] = 100 mg L^{-1}, dose = 3.0 mg, v = 5 mL, pH = 3, T = 25 ℃) form aqueous solution. **e** Effect of interfering ions on the removal percent and distribution coefficient of LaIII) and Pr(III) from a synthetic solution containing Ca(II), Sr(II), Cd(II) and Cs(I) ions (t = 1 min, [M] = 100 mg L^{-1}, dose = 5 mg, v = 5 mL, pH = 3, T = 25 ℃). **f** The influence of the number of the reuse cycles of the GO-imidazole-FeCN on the removal percentage of La(III) (t = 1 min, [La] = 100 mg L^{-1}, dose = 5 mg, v = 5 mL, pH = 3, T = 25 ℃) and Pr(III) ([Pr] = 100 mg L^{-1}, dose = 5 mg, V = 5 mL, pH = 3, T = 25 ℃) from aqueous media

available binding sites for the contaminated species can be enhanced.

Effect of solution temperature

The effect of temperature on La(III) and Pr(III) ions adsorption by GO-imidazole-FeCN was studied in the range of 25–65 ℃, as described in Fig. 5c. The capture performances of both studied metal ions enhanced with further increase in the temperature of adsorption solution media, i.e., endothermic adsorption reaction. The preferential adsorption of metal ions at high temperatures indicates that the viscosity of the adsorption solution is reduced, and the metal ion diffusion is enhanced from the bulk of the solution to the binding sites on the adsorbent surface. Thus, the metal ion species were very close to the active sites.

Thermodynamic parameter ($\Delta G°$) and ($\Delta H°$ and $\Delta S°$) values were calculated from the slope and intercept of the linear plot of Ln K_d against T^{-1} (Table S1), as described in Fig. 5d. The values of these factors are listed in Table 2. The negative values of $\Delta G°$ indicated that the adsorption of both La(III) and Pr(III) on GO-imidazole-FeCN is available and spontaneous. The positive values of $\Delta H°$ and $\Delta S°$ confirm that the adsorption process is an endothermic reaction and irreversibility and stabilized the sorption reaction (Sahmoune 2019).

Table 1 Linearized adsorption isotherm constants and R^2 values for La(III) and Pr(III) sorption onto the GO-imidazole-FeCN

Isotherm	Parameters	Metal ions	
		La(III)	Pr(III)
Langmuir	Qo (mg/g)	781.25	862.07
	b (ml/mg)	16.03×10^{-3}	32.78×10^{-3}
	R_L	0.384	0.234
	R^2	0.985	0.998
Freundlich	K_f (mg/g)	46.464	98.20
	n	2.10	2.61
	R^2	0.922	0.930
Dubinin–Radushkevich	q_m	16.99	15.511
	β	0.00527	0.00403
	R^2	0.949	0.961
	E_{DR}	9.74	11.139
Tempkin	K_T	0.1424	0.3678
	B	177.173	172.729
	R^2	0.939	0.967
Elvoich	q_m	440.53	156.99
	K_e	1.006	1.018
	R^2	0.857	0.900
Redlich-peterson	B (L/mg)	0.52306	0.61688
	A (L/g)	46.46	98.216
	R^2	0.935	0.972
Harkins–Jura	B_{HJ}	2.44	2.395
	A_{HJ}	40,772.06	74,748.47
	R^2	0.7443	0.7184
Sips	n	0.946	0.974
	b_s		
	R^2	0.945	0.977
Halsey	n_H	−2.10	−2.61
	K_H	3.19×10^{-4}	6.321×10^{-6}
	R^2	0.923	0.930
Jovanovich	q_{max}	247.25	327.95
	K_j	−0.00336	−0.00328
	R^2	0.564	0.516
q_{exp}, mg/g		785.55	867.67

Table 2 Thermodynamic parameters for sorption of La(III) and Pr(III) ions

Metal ions	T (K)	$\Delta G°$ (k J mole^{-1})	$\Delta H°$ (k J mole^{-1})	$\Delta S°$ (J mole^{-1} K^{-1})
La(III)	298	−27.09	32.61	200.33
	308	−29.09		
	318	−31.095		
	328	−33.10		
	338	−35.10		
Pr(III)	298	−28.86	37.033	221.11
	308	−31.07		
	318	−33.28		
	328	−35.49		
	338	−37.70		

Effect of interfering ions on the sorption of La(III) and Pr(III)

The effect of interfering ions, which are present in fission products and radioactive waste, on the sorption of La(III) and Pr(III) was studied, as shown in Fig. 5e. For this objective, 10.0 mL of aqueous solutions containing an equivalent concentration (100 mg/L) of La(III), Pr(III), Ca(II), Sr(II), Cd(II), and Cs(I) ions were prepared. The experiment was performed by mixing 5 mL of synthetic solution with 10 mg of GO-imidazole-FeCN, contact time 1 min, pH 3, and v/m 0.50 L g^{-1}. The distribution coefficient (K_d) and the removal percent of the studied metal ions were investigated as shown in Fig. 5e, and separation factors (SF) were calculated and are summarized in Table S3. The K_d values for La(III) and Pr(III) were 0.643 and 1.441 L g^{-1}, respectively, and compared to that of different interfering ions, which was less than 0.191 L g^{-1}. However, further work is required to get more assessment for using these materials. Moreover, the separation factor of La(III) and Pr(III) from different metal ions is higher than 4.20, see Table S3. As a result, this GO-imidazole-FeCN might be a strategic adsorbent for the sorption and possible separation of La(III) and Pr(III) from some fission products.

Recoverability and reusability studies

In this section, the recoverability and reusability of the GO-imidazole-FeCN/M complex (M = La(III) or Pr(III)) are investigated. In this regard, the GO-imidazole-FeCN/M complex was treated with a 5.0 mL aqueous solution of 0.5 M HCl. Then, it was filtrated and redispersed in a 5 mL aqueous solution of 0.5 M $K_4[Fe(CN)_6]$ for 30.0 min. Finally, the obtained solid filtrate was washed three times with distilled water for the next reuse. Fifth, the adsorbent was regenerated-reuse under the conditions applied as in first time. As presented in Fig. 5f, the adsorption slightly changes over the five reuse runs. This change demonstrated the high stability and efficiency of the constructer adsorbent.

Adsorption mechanism

Here, as previously explained in Scheme 1, the surface of GO was modified with quaternary amine through a reaction with 1-methyl imidazole in the presence of epichlorohydrin. Moreover, the positive amine formed was neutralized with a negative chlorine anion (GO-imidazole-Cl) (refer to Sect. 3.1.2. and 3.1.5). In order to improve the affinity of the composite towards the metal ions, the Cl^- was substituted with $K_3[Fe(CN)_6]^-$ through the reaction of GO-imidazole-Cl

Table 3 Comparison of La(III) and Pr(III) adsorption in different types of adsorbents

Metal ion	Adsorbent	Q_o, mg/g	References
La(III)	GO-imidazole-FeCN	785.55	This work
	GO-$TAPA_{1:2}$ composite	11.24	(Zhao et al. 2021)
	Nanogoethite (NG)	52.5	(Sayed et al. 2021)
	Activated carbon@goethite (GAC-1)	57.7	(Sayed et al. 2021)
	Sodium alginate@goethite (GSA-2)	79.1	(Sayed et al. 2021)
	PA-MNPs	18.4	(Gaete et al. 2021)
	C272-MNPs	6.6	(Molina et al. 2019)
	C301-MNPs	7.6	(Molina et al. 2019)
	D2PA-MNPs	8.3	(Molina et al. 2019)
	Bio-templated chiral nematic mesoporous silica films (MSFs-1)	77.74	(Liu et al. 2019)
	Bio-templated chiral nematic mesoporous silica films (MSFs-2)	69.24	(Liu et al. 2019)
	GA-g-PAM/SiO_2	7.9	(Iftekhar et al. 2018)
	(CTS/PVA/TMPTMS)	263.16	(Najafi et al. 2018)
	$CuFe_2O_4$	42.02	(Tu and Johnston 2018)
	Fe_3O_4@TiO_2@P_20_4 nanoparticles	8.51	(Yan et al. 2017)
	Graphene oxide nanosheets	85.67	(Ashour et al. 2017)
	Polyethylenimine sodium phosphonate resin (PEIPR-Na)	1.06	(Bendia et al. 2017)
	Cys-Fe_3O_4 NPs	71.5	(Ashour et al. 2016)
	Silica SBA-15/tungstophosphate	11.60	(Ahmadi et al. 2016)
	Clay minerals	1.73	(Yanfei et al. 2016)
	CTS-g-PAA/APT composite	333.33	(Zhu et al. 2015)
	Fe_3O_4/chitosan nanocomposite	153.8	(Haldorai et al. 2015)
	Cysteine-functionalized chitosan magnetic nano-based particles	17.9	(Galhoum et al. 2015)
	Lewatit TP 260	106.7	(Esma et al. 2014)
	Lewatit TP 207	114.7	(Esma et al. 2014)
	Fe_3O_4@SiO_2@polyaniline-graphene oxide	15.50	(Su et al. 2014)
	Magnetic ZnO clay nanocomposite hydrogel	58.84	(Zheng et al. 2014)
	Fish scale	200	(Das et al. 2014)
	Neemsawdust	160.2	(Das et al. 2014)
	SnO_2–TiO_2nanocomposites	65.6	(Rahman et al. 2014)
	Magnetic GMZ bentonite	18.4	(Wu et al. 2012)
	Magnetic alginate–chitosan gel beads	97.1	(Wu et al. 2011)
	Iron oxide-loaded calcium alginate beads	123.5	(Wu et al. 2010)
	Alkyl phosphinic acid resin	1.99	(Fu et al. 2007)
	Multiwalled carbon nanotubes	8.30	(Liang et al. 2005)
	8-quinolinole-immobilized fluorinated metal alkoxide glass	8.33	(Kajiya et al. 2004)
Pr(III)	GO-imidazole-FeCN	867.67	This work
	Hydrophobic ionic liquid (IL5)	141.5	(Devanathan et al. 2021)
	Algal/poly(ethyleneimine) (PEI) beads (APEI)	105.68	(He et al. 2021)
	Phosphorylation of APEI activated beads (P2-APEI)	301.55	(He et al. 2021)
	polysulfoneimmobilized Turbinaria conoides	160.64	(Rangabhashiyam et al. 2021)
	PA-MNPs	17.6	(Gaete et al. 2021)
	Transcarpathian clinoptilolite	280.0	(Stashkiv et al. 2019)
	C272-MNPs	7.7	(Molina et al. 2019)
	C301-MNPs	8.2	(Molina et al. 2019)
	D2PA-MNPs	8.7	(Molina et al. 2019)
	Laminaria digitata beads	125.4	(Wang et al. 2017)

Table 3 (continued)

Metal ion	Adsorbent	Q_o, mg/g	References
	Laminaria digitata foams	111.3	(Wang et al. 2017)
	Polyethylenimine sodium phosphonate resin (PEIPR-Na)	6.23	(Bendia et al. 2017)
	Fe_3O_4@TiO_2@P_20_4 nanoparticles	10.2	(Yan et al. 2017)
	DTPA-functionalized magnetic nanosorbents	0.616	(Zhang et al. 2016)
	polysulfone immobilized T. conoides (PITC)	119.5	(Vijayaraghavan and Jegan 2015)
	Turbinaria conoides	146.4	(Vijayaraghavan and Jegan 2015)
	Silica gel/diglycol amic acid	12.72	(Ogata et al. 2015)
	Fe_3O_4@SiO_2@polyaniline-graphene oxide	11.1	(Su et al. 2014)
	Clinoptilolite-containing tuff	17.75	(Kozhevnikova 2012)
	D72 resin (–SO_3H)	294	(XIONG et al. 2012)
	SBA-15/aurintricarboxylic acid	2.0	(Mallah et al. 2010)
	Alkyl phosphinic acid resin	2.03	(Fu et al. 2007)
	TVEX–PHOR resin	49.0	(El-Dessouky et al. 2007)
	DMDOHEMA impregnated resin	0.11	(Van Hecke and Modolo 2004)
	TODGA impregnated resin	0.06	(Van Hecke and Modolo 2004)

with $K_4[Fe(CN)_6]$ to form GO-imidazole-FeCN and release KCl (refer to Sect. 3.1.2. and 3.1.5). Potassium ferricyanide anion was arranged, as shown in Fig. S4. Briefly, the six (CN) groups are arranged in a hexagonal configuration; the Fe-atom is linked with three N-atoms, and three K-atoms interact with the other remaining N-atom (Getman 1921). Upon interaction with the M-ion, the K-atoms can be replaced with the M-ions; hence, K-atoms will be liberated into the bulk of the solution as presented in Fig. S4. In order to confirm this suggestion, the concentrations of potassium in the solution after the adsorption process were determined. The presence of potassium ions in the adsorption solution was noted. This explains that the adsorption process of both La(III) and Pr(III) occurs by substituting potassium ions from ferrocyanide. After that, the released potassium can form KOH in the aqueous solution, leading to an increase in the value of solution pH (see Fig. 4c). Also, the mechanism was supported by the EDS analysis (Sect. 3.1.5., Fig. S2). Moreover, the FTIR analysis of GO-imidazole-FeCN after adsorption of both La(III) and Pr(III) (Sect. 3.1.3, Fig. S5) showed enhancement of the bands related to the water vibration motions at 3430 and 1575 cm^{-1} and M–O bond vibration at 464 cm^{-1} which suppose that the GO-imidazole-FeCN-M complex was stabilized with water molecules.

Comparison with other adsorbent material

A comparison of the sorption capacities of La(III) and Pr(III) on GO-imidazole-FeCN with several adsorbents is shown in Table 3. The comparative results reported that the GO-imidazole-FeCN resulted in rapid adsorption kinetics and higher sorption capacity than other adsorbents. Therefore, GO-imidazole-FeCN could be applied as a highly efficient adsorbent for the sorption of La(III) and Pr(III) from aqueous solutions.

Conclusion

In this paper, GO-imidazole-FeCN composite was utilized to investigate the sorption of Pr(III) and La(III) from an aqueous solution using a batch adsorption process. The experimental results showed that the sorption is comparatively fast, reaching equilibrium in 1 min for studied metal ions. The thermodynamic results indicated that the sorption process was endothermic and spontaneous. Moreover, the sorption isotherms obeyed the Langmuir model in terms of the equilibrium sorption capacities of La(III) and Pr(III). The experimental sorption capacities were 785.55 and 867.67 mg/g for La(III) and Pr(III), respectively. GO-imidazole-FeCN has an excellent regeneration-reused behavior.

Supplementary Information The online version contains supplementary material available at https://doi.org/10.1007/s13201-023-01955-w.

Acknowledgements Not applicable.

Funding Open access funding provided by The Science, Technology & Innovation Funding Authority (STDF) in cooperation with The Egyptian Knowledge Bank (EKB). Open access funding provided by The Science, Technology & Innovation Funding Authority (STDF) in cooperation with The Egyptian Knowledge Bank (EKB).

Data availability All data generated or analyzed during this study are included in this published article and its supplementary information files.

Declarations

Conflict of interest The authors declare no competing interests.

Consent for publication All authors approved the paper submission.

Ethics approval and consent to participate Not applicable.

References

Ahmadi M, Yavari R, Faal AY, Aghayan H (2016) Preparation and characterization of titanium tungstophosphate immobilized on mesoporous silica SBA-15 as a new inorganic composite ion exchanger for the removal of lanthanum from aqueous solution. J Radioanal Nucl Chem 310(1):177–190. https://doi.org/10.1007/s10967-016-4748-y

Ashour RM, Abdel-Magied AF, Abdel-Khalek AA, Helaly OS, Ali MM (2016) Preparation and characterization of magnetic iron oxide nanoparticles functionalized by l-cysteine: Adsorption and desorption behavior for rare earth metal ions. J Environ Chem Eng 4(3):3114–3121. https://doi.org/10.1016/j.jece.2016.06.022

Ashour RM, Abdelhamid HN, Abdel-Magied AF, Abdel-Khalek AA, Ali MM, Uheida A, Dutta J (2017) Rare earth ions adsorption onto graphene oxide nanosheets. Solvent Extr Ion Exch 35(2):91–103. https://doi.org/10.1080/07366299.2017.1287509

Baranitharan P, Ramesh K, Sakthivel R (2019) Analytical characterization of the Aegle marmelos pyrolysis products and investigation on the suitability of bio-oil as a third generation bio-fuel for CI engine. Environ Prog Sustain Energy 38(4):13116

Barroso-Bogeat A, Alexandre-Franco M, Fernandez-Gonzalez C, Gomez-Serrano V (2019) Activated carbon surface chemistry: changes upon impregnation with Al(III), Fe(III) and Zn (II)-metal oxide catalyst precursors from $NO3^-$ aqueous solutions. Arab J Chem 12(8):3963–3976. https://doi.org/10.1016/j.arabjc.2016.02.018

Behdani FN, Rafsanjani AT, Torab-Mostaedi M, Mohammadpour SMAK (2013) Adsorption ability of oxidized multiwalled carbon nanotubes towards aqueous Ce(III) and Sm(III). Korean J Chem Eng 30(2):448–455. https://doi.org/10.1007/s11814-012-0126-9

Bendia H, Abderrahim O, Villemin D, Didi MA (2017) Studies on the feasibility of using a novel phosphonate resin for the separation of U (VI), La(III) and Pr(III) from aqueous solutions. J Radioanal Nucl Chem 312(3):587–597. https://doi.org/10.1007/s10967-017-5244-8

Das D, Varshini CJS, Das N (2014) Recovery of lanthanum(III) from aqueous solution using biosorbents of plant and animal origin: Batch and column studies. Miner Eng 69:40–56. https://doi.org/10.1016/j.mineng.2014.06.013647

Devanathan R, Balaji GL, Lakshmipathy R (2021) Adsorption of rareearth Ce^{3+} and Pr^{3+} ions by hydrophobic ionic liquid. J Environ Public Health. https://doi.org/10.1155/2021/6612500

Dong Z, Zhao L (2018) Surface modification of cellulose microsphere with imidazolium-based ionic liquid as adsorbent: effect of anion variation on adsorption ability towards Au(III). Cellulose 25(4):2205–2216. https://doi.org/10.1007/s10570-018-1735-1

El-Dessouky SI, El-Sofany EA, Daoud JA (2007) Studies on the sorption of praseodymium(III), holmium(III) and cobalt (II) from nitrate medium using TVEX–PHOR resin. J Hazard Mater 143(1–2):17–23. https://doi.org/10.1016/j.jhazmat.2006.08.070

Esma B, Omar A, Amine DM (2014) Comparative study on lanthanum(III) sorption onto Lewatit TP 207 and Lewatit TP 260. J Radioanal Nucl Chem 299(1):439–446. https://doi.org/10.1007/s10967-013-2766-6

Favre-Reguillon A, Draye M, Cote G, Czerwinsky KR (2019) Insights in uranium extraction from spent nuclear fuels using dicyclohexano-18-crown-6–Fate of rhenium as technetium homolog. Sep Purif Techn 209:338–434. https://doi.org/10.1016/j.seppur.2018.07.034

Fu Q, Yang L, Wang Q (2007) On-line preconcentration with a novel alkyl phosphinic acid extraction resin coupled with inductively coupled plasma mass spectrometry for determination of trace rare earth elements in seawater. Talanta 72(4):1248–1254. https://doi.org/10.1016/j.talanta.2007.01.015

Gaete J, Molina L, Valenzuela F, Basualto C (2021) Recovery of lanthanum, praseodymium and samarium by adsorption using magnetic nanoparticles functionalized with a phosphonic group. Hydrometallurgy, 105698. https://doi.org/10.1016/j.hydromet.2021.105698

Galhoum AA, Mafhouz MG, Abdel-Rehem ST, Gomaa NA, Atia AA, Vincent T, Guibal E (2015) Cysteine-functionalized chitosan magnetic nano-based particles for the recovery of light and heavy rare earth metals: uptake kinetics and sorption isotherms. Nanomaterials 5(1):154–179. https://doi.org/10.3390/nano5010154

Getman FH (1921) A study of the absorption spectra of potassium ferro- and ferricyanides. J Phys Chem 25(2):147–159

Haldorai Y, Rengaraj A, Ryu T, Shin J, Huh YS, Han YK (2015) Response surface methodology for the optimization of lanthanum removal from an aqueous solution using a Fe_3O_4/chitosan nanocomposite. Mater Sci Eng, B 195:20–29. https://doi.org/10.1016/j.mseb.2015.01.006

He C, Salih KA, Wei Y, Mira H, Abdel-Rahman AAH, Elwakeel KZ, Hamza MF, Guibal E (2021) Efficient recovery of rare earth elements (Pr(III) and Tm(III)) from mining residues using a new phosphorylated hydrogel (Algal Biomass/PEI). Metals 11(2):294. https://doi.org/10.3390/met11020294

Huo JB, Yu G, Wang J (2021) Adsorptive removal of Sr (II) from aqueous solution by polyvinyl alcohol/graphene oxide aerogel. Chemosphere 278:130492. https://doi.org/10.1016/j.chemosphere.2021.130492

Iftekhar S, Srivastava V, Casas A, Sillanpää M (2018) Synthesis of novel GA-g-PAM/SiO2 nanocomposite for the recovery of rare earth elements (REE) ions from aqueous solution. J Clean Prod 170:251–259. https://doi.org/10.1016/j.jclepro.2017.09.166

Kajiya T, Aihara M, Hirata S (2004) Determination of rare earth elements in seawater by inductively coupled plasma mass spectrometry with on-line column pre-concentration using 8-quinolinole-immobilized fluorinated metal alkoxide glass. Spectrochim Acta Part B 59(4):543–550. https://doi.org/10.1016/j.sab.2003.12.019

Kozhevnikova NM (2012) Sorption of praseodymium(III) ions from aqueous solutions by a natural clinoptilolite-containing tuff. Russ

J Phys Chem A 86(1):127–130. https://doi.org/10.1134/S0036024412010177

Lei Y, Yang G, Huang Q, Dou J, Dai L, Deng F, Liu M, Li X, Zhang X, Wei Y (2022) Facile synthesis of ionic liquid modified silica nanoparticles for fast removal of anionic organic dyes with extremely high adsorption capacity. J Mol Liq 347:117966

Liang P, Liu Y, Guo L (2005) Determination of trace rare earth elements by inductively coupled plasma atomic emission spectrometry after preconcentration with multiwalled carbon nanotubes. Spectrochim Acta Part B 60(1):125–129. https://doi.org/10.1016/j.sab.2004.11.010

Liu E, Chen L, Dai J, Wang Y, Li C, Yan Y (2019) Fabrication of phosphate functionalized chiral nematic mesoporous silica films for the efficient and selective adsorption of lanthanum ions. J Mol Liq 277:786–793. https://doi.org/10.1016/j.molliq.2019.01.032

Liu Y, Shi Y, Cui Y, Zhao F, Chen M (2022) Design and preparation of imidazole ionic liquid-based magnetic polymers and its adsorption on sunset yellow dye. Mater 15(7):2628

Lou Z, Xing S, Xiao X, Shan W, Xiong Y, Fan Y (2018) Selective adsorption of Re (VII) by chitosan modified with imidazolium-based ionic liquid. Hydrometall 179:141–148

Mallah M, Maragheh GM, Badiei A, Habibzadeh SR (2010) Novel functionalized mesopore of SBA-15 as prospective sorbent for praseodymium and lutetium. J Radioanal Nucl Chem 283(3):597–601. https://doi.org/10.1007/s10967-010-0452-5

Molina L, Gaete J, Alfaro I, Ide V, Valenzuela F, Parada J, Basualto C (2019) Synthesis and characterization of magnetite nanoparticles functionalized with organophosphorus compounds and its application as an adsorbent for La(III), Nd(III) and Pr(III) ions from aqueous solutions. J Mol Liq 275:178–191. https://doi.org/10.1016/j.molliq.2018.11.074

Najafi LM, Keshtkar AR, Moosavian MA (2018) Adsorption of cerium and lanthanum from aqueous solutions by chitosan/polyvinyl alc ohol/3mercaptopropyltrimethoxysilane beads in batch and fixed-bed systems. Part Sci Technol 36(3):340–350. https://doi.org/10.1080/02726351.2016.1248262

Naushad M, Ahamad T, Khan MR (2021) Fabrication of magnetic nanoparticles supported ionic liquid catalyst for trans-esterification of vegetable oil to produce biodiesel. J Mol Liq 330:115648

Ogata T, Narita H, Tanaka M (2015) Adsorption behavior of rare earth elements on silica gel modified with diglycolamic acid. Hydrometallurgy 152:178–182. https://doi.org/10.1016/j.hydromet.2015.01.005

Pepper SE, Ogden MD (2013) Perrhenate extraction studies by Cyphos 101-IL; screening for implementation in technetium removal. Sep Purif Techn 118:847–852. https://doi.org/10.1016/j.seppur.2013.08.029

Rahman MM, Khan SB, Marwani HM, Asiri AM (2014) SnO_2–TiO_2 nanocomposites as new adsorbent for efficient removal of La(III) ions from aqueous solutions. J Taiwan Inst Chem Eng 45(4):1964–1974. https://doi.org/10.1016/j.jtice.2014.03.018

Rangabhashiyam S, Vijayaraghavan K, Jawad AH, Singh P (2021) Sustainable approach of batch and continuous biosorptive systems for praseodymium and thulium ions removal in mono and binary aqueous solutions. Environ Technol Innovat 23:101581. https://doi.org/10.1016/j.eti.2021.101581

Ronda CR, Jüstel T, Nikol H (1998) Rare earth phosphors: fundamentals and applications. J Alloy Compd 275:669–676. https://doi.org/10.1016/s0925-8388(98)00416-2

Sahmoune MN (2019) Evaluation of thermodynamic parameters for adsorption of heavy metals by green adsorbents. Environ Chem Lett 17(2):697–704. https://doi.org/10.1007/s10311-018-00819-z

Sayed MA, Aly HF, Mahmoud HH, Abdelwahab SM, Helal AI, Wilson LD (2021) Design of hybrid goethite nanocomposites as potential sorbents for lanthanum from aqueous media. Sep Sci Technol 56(17):2865–2879. https://doi.org/10.1080/01496395.2020.1853168

Singh JK, Sharma RK, Ghosh P, Kumar A, Khan ML (2018) Imidazolium based ionic liquids: a promising green solvent for water hyacinth biomass deconstruction. Front Chem 6:548. https://doi.org/10.3389/fchem.2018.00548

Stashkiv O, Vasylechko V, Gryshchouk G, Patsay I (2019) Solid phase extraction of trace amounts of praseodymium using transcarpathian clinoptilolite. Colloids Interfaces 3(1):27. https://doi.org/10.3390/colloids3010027

Su S, Chen B, He M, Hu B, Xiao Z (2014) Determination of trace/ultratrace rare earth elements in environmental samples by ICP-MS after magnetic solid phase extraction with Fe_3O_4@ SiO_2@ polyaniline–graphene oxide composite. Talanta 119:458–466. https://doi.org/10.1016/j.talanta.2013.11.027

Subasree N, Selvi JA (2020) Imidazolium based ionic liquid derivatives; synthesis and evaluation of inhibitory effect on mild steel corrosion in hydrochloric acid solution. Heliyon 6(2):e03498

Tadjarodi A, Jalalat V, Zare-Dorabei R (2015) Adsorption of La(III) in aqueous systems by N-(2-hydroxyethyl) salicylaldimine-functionalized mesoporous silica. Mater Res Bull 61:113–119. https://doi.org/10.13140/RG.2.1.4050.1601

Tu YJ, Johnston CT (2018) Rapid recovery of rare earth elements in industrial wastewater by CuFe2O4 synthesized from Cu sludge. J Rare Earths 36(5):513–520. https://doi.org/10.1016/j.jre.2017.11.009

Van Hecke K, Modolo G (2004) Separation of actinides from low level liquid wastes (LLLW) by extraction chromatography using novel DMDOHEMA and TODGA impregnated resins. J Radioanal Nucl Chem 261(2):269–275. https://doi.org/10.1023/B:JRNC.0000034858.26483.ae

Vijayaraghavan K, Jegan J (2015) Entrapment of brown seaweeds (*Turbinaria conoides* and *Sargassum wightii*) in polysulfone matrices for the removal of praseodymium ions from aqueous solutions. J Rare Earths 33(11):1196–1203. https://doi.org/10.1016/S1002-0721(14)60546-9

Wang S, Hamza MF, Vincent T, Faur C, Guibal E (2017) Praseodymium sorption on Laminaria digitata algal beads and foams. J Colloid Interface Sci 504:780–789. https://doi.org/10.1016/j.jcis.2017.06.028

Wu D, Zhao J, Zhang L, Wu Q, Yang Y (2010) Lanthanum adsorption using iron oxide loaded calcium alginate beads. Hydrometallurgy 101(1–2):76–83. https://doi.org/10.1016/j.hydromet.2009.12.00

Wu D, Zhang L, Wang L, Zhu B, Fan L (2011) Adsorption of lanthanum by magnetic alginate-chitosan gel beads. J Chem Technol Biotechnol 86(3):345–352. https://doi.org/10.1002/jctb.2522

Wu D, Zhu C, Chen Y, Zhu B, Yang Y, Wang Q, Ye W (2012) Preparation, characterization and adsorptive study of rare earth ions using magnetic GMZ bentonite. Appl Clay Sci 62:87–93. https://doi.org/10.1016/j.clay.2012.04.015

Xie K, Dong Z, Wang N, Qi W, Zhao L (2021) Radiation synthesis of imidazolium-based ionic liquid modified silica adsorbents for ReO 4− adsorption. New J Chem 45(17):7659–7670

Xin B, Hao J (2014) Imidazolium-based ionic liquids grafted on solid surfaces. Chem Soc Rev 43(20):7171–7187. https://doi.org/10.1039/c4cs00172a

Xiong C, Jingfei ZHU, Chen SHEN, Qing CHEN (2012) Adsorption and desorption of praseodymium(III) from aqueous solution using D72 resin. Chin J Chem Eng 20(5):823–830. https://doi.org/10.1016/S1004-9541(12)60405-4

Xu C, Qu X (2014) Cerium oxide nanoparticle: a remarkably versatile rare earth nanomaterial for biological applications. NPG Asia Materials 6(3):e90–e90. https://doi.org/10.1038/am.2013.88

Yan P, He M, Chen B, Hu B (2017) Fast preconcentration of trace rare earth elements from environmental samples by di (2-ethylhexyl) phosphoric acid grafted magnetic nanoparticles followed by inductively coupled plasma mass spectrometry detection. Spectrochim Acta Part B 136:73–80. https://doi.org/10.1016/j.sab.2017.08.011

Yanfei XIAO, Huang L, Zhiqi LONG, Zongyu FENG, Liangshi WANG (2016) Adsorption ability of rare earth elements on clay minerals and its practical performance. J Rare Earths 34(5):543–548. https://doi.org/10.1016/S1002-0721(16)60060-1

Zhang Z, Wang Z, Chen D, Miao R, Zhu Q, Zhang X, Zhou L, Li ZA (2014) Purification of praseodymium to 4N5+ purity. Vacuum 102:67–71. https://doi.org/10.1016/j.vacuum.2013.11.008

Zhang H, McDowell RG, Martin LR, Qiang Y (2016) Selective extraction of heavy and light lanthanides from aqueous solution by advanced magnetic nanosorbents. ACS Appl Mater Interfaces 8(14):9523–9531. https://doi.org/10.1021/acsami.6b01550

Zhao Z, Sun X, Dong Y, Wang Y (2016) Synergistic effect of acid–base coupling bifunctional ionic liquids in impregnated resin for rare earth adsorption. ACS Sustain Chem Engin 4(2):616–624

Zhao X, Jiang X, Peng D, Teng J, Yu J (2021) Behavior and mechanism of graphene oxide-tris (4-aminophenyl) amine composites in adsorption of rare earth elements. J Rare Earths 39(1):90–97. https://doi.org/10.1016/j.jre.2020.02.006

Zheng X, Wu D, Su T, Bao S, Liao C, Wang Q (2014) Magnetic nanocomposite hydrogel prepared by ZnO-initiated photopolymerization for La(III) adsorption. ACS Appl Mater Interfaces 6(22):19840–19849. https://doi.org/10.1021/am505177c

Zhu Y, Zheng Y, Wang A (2015) Preparation of granular hydrogel composite by the redox couple for efficient and fast adsorption of La(III) and Ce(III). J Environ Chem Eng 3(2):1416–1425. https://doi.org/10.1016/j.jece.2014.11.028

Zsabka P, Van Hecke K, Adriaensen L, Wilden A, Modolo G, Verwerft M, Binnemans K, Cardinaels T (2018) Solvent extraction of Am(III), Cm(III), and Ln(III) ions from simulated highly active raffinate solutions by TODGA diluted in Aliquat-336 nitrate ionic liquid. Solv Extract Ion Exch 36(6):519–541. https://doi.org/10.1080/07366299.2018.1545288

Zuo L, Yu S, Zhou H, Jiang J, Tian X (2011) Adsorption of Eu(III) from aqueous solution using mesoporous molecular sieve. J Radioanal Nucl Chem 288(2):579–586. https://doi.org/10.1007/s10967-010-0972-z